HIGH-RESOLUTION NEURAL NETWORK PROCESSING OF LFM RADAR PULSES

Jabran Akhtar

Norwegian Defence Research Establishment (FFI), Kjeller, Norway, jabran.akhtar@ffi.no

ABSTRACT

In radar applications, the bandwidth of a transmitted pulse determines the range resolution and the ability to disclose densely spaced targets. The processing of radar signals is often carried out through matched filtering (MF) which aims to maximize the signal to noise ratio. This work presents an alternative processing scheme for oversampled radar signals based on small-sized neural networks. The networks are trained with an objective to return MF outcomes corresponding to a higher bandwidth pulse. The article demonstrates how such a neural network design can be constructed and compares against traditional processing and detection.

Index Terms— Matched filter, pulse compression, mismatched filter, neural networks, LFM, CFAR

1. INTRODUCTION

Transmission and reception of signals is a basic fundamental process of any active radar system. The shape and form of the pulses subsequently plays a key role in determining the overall system performance of a radar setup. Particularly, the bandwidth of the applied waveform is an important parameter in pulse compression as this regulates the range resolution and ability to distinguish between densely spaced targets [1]. .

A popular class of radar waveform often employed in radars are linear frequency modulated (LFM) pulses who have been studied extensively over the years [1]. LFM pulses sweep a desired bandwidth and provide high range resolution decoupled with the duration of the pulse. The incoming reflections may be processed through matched filtering (MF) which is an optimal solution with respect to signal to noise ratio (SNR). There is thus no advantage in trying to replicate MF with neural networks (NN), however, alternatives to MF, often denoted as mismatched filtering or least-square estimation methods, are known techniques and can be used to e.g. control the sidelobe levels at the expense of other properties [2, 3, 4, 5]. A NN can conceivably be implemented to perform mismatched filtering given specific optimization requirements. Although machine learning has been in much focus over the years there has been limited research on this topic as most of emphasis has been on target detection and classification where underlying radar processing has already been carried out [6, 7, 8].

In a related work [9] it is shown that the resolution of incoming LFM radar signals can be enhanced using machine learning methods. The proposed method, however, relied on processing of signals bin by bin with significant computational complexity. This work can be seen complementing the previous paper as processing of the full signal is now proposed carried out in a single step which corresponds directly to a frequency domain type of approach. To evaluate the outcomes, the paper presents simulation results including constant false alarm rate (CFAR) [10] target detection tests illustrating an improvement with the incorporation of a trained neural network.

2. SYSTEM MODEL

A standard radar model is assumed where an LFM pulse is transmitted at regular intervals. The pulse is defined as

$$p(t) = \exp\left(j2\pi((f_0 - \frac{\Delta f}{2})t + \frac{\Delta f}{2T}t^2)\right), \qquad (1)$$

where f_0 is the carrier frequency and Δf is the bandwidth. The pulse starts at $t = 0$ and terminates at $t = T$. The receiving signal containing N target reflections may thus be characterized as

$$s(t) = \sum_{l=1}^{N} \rho_n p(t - \Delta_n) e^{j2\pi\nu_l t} + z(t) \qquad (2)$$

where Δ_n corresponds to the delay of reflector l, ρ_n are complex-valued reflection coefficients, ν_l corresponds to frequency shift due to target velocity and $z(t)$ is white Gaussian noise. The radar is set to cover a certain range up to r_{max} and the incoming data is collected with R number of samples after emission of each pulse. In vector notation, the discrete sampled pulse $p(t)$ is assumed to consist of L samples and is denoted by $\mathbf{p} \in \mathbb{C}^L$ while the sampled signal (2) is indicated by $\mathbf{s} \in \mathbb{C}^R$. For simplicity, but without loss of generality, in the following the aspects behind downsampling and baseband conversion are ignored. The sampling rate of the radar system is given by f_s and is set to satisfy $f_s > 2\Delta f$. As typical for many modern systems, the sampling rate may be significantly higher as oversampling is often employed.

In the main processing step, a MF operation is assumed carried out on the receiving data using the conjugated and time-reversed discrete version of the emit pulse, $\mathbf{p}^*$. This pulse may optionally be tapered with a windowing function

Dette er en postprint-versjon/This is a postprint version.
DOI til publisert versjon/DOI to published version: 10.1109/ICASSP49357.2023.10095034

to control the sidelobes [11, 12] and is denoted by $\mathbf{p}_w^*$, resulting in the outcome $\mathbf{y} = \mathbf{s} * \mathbf{p}_w^* = r(\mathbf{s}) \quad \in \mathbb{C}^R$, where $*$ is the convolution operator. This is a standard technique for pulse compression and normally carried out in frequency domain for computational reasons. This procedure can also be expressed through the use of the operator function $r : \mathbf{s} \rightarrow \mathbf{y}$ which takes as the input sampled signal and returns the output assuming the matched filter is given. The range resolution of this system is determined by the bandwidth of the emit signal, $\Delta R = \frac{c}{2\Delta f}$ where c is the speed of propagation. In order to improve the resolution, a higher bandwidth pulse is normally required. To model an identical system but with greater bandwidth, a different version of the radar setup can be formed where the employed pulse is replaced by

$$\hat{p}(t) = \exp\left(j2\pi((f_0 - \frac{\Delta\hat{f}}{2})t + \frac{\Delta\hat{f}}{2T}t^2)\right), \tag{3}$$

where $\Delta\hat{f} > \Delta f$; however, where the sampling rate of the system still satisfies $f_s > 2\Delta\hat{f}$. The equivalent MF output can be specified as $\hat{\mathbf{y}} = \hat{\mathbf{s}} * \hat{\mathbf{p}}_w^* = \hat{r}(\hat{\mathbf{s}}) \quad \in \mathbb{C}^R$. This can be instituted as a complex function $\hat{r} : \hat{\mathbf{s}} \rightarrow \hat{\mathbf{y}}$ where $\hat{\mathbf{p}}_w^*$ is the discrete conjugated and time-reversed higher bandwidth pulse with an optionally applied apodization function. As long as the radar transmits standard bandwidth pulses $\mathbf{p}$, yet with a larger receiver sampling rate, the receiver output processing can suppositionally be altered to simulate the use of a high resolution pulse. This can be treated as a mismatched filtering technique where the aim is not to directly maximize the SNR rather to replicate the output towards a modified super-resolution filter response.

Taking account of the notes above, one can propose to construct a new function $r_{NN} : \mathbf{s} \rightarrow \dot{\mathbf{y}}$ which takes the sampled input data based on the low bandwidth pulse $\mathbf{p}$ and attempts to yield an output $\dot{\mathbf{y}}$, $\dot{\mathbf{y}} \approx \hat{\mathbf{y}}$, approximating the greater bandwidth pulse, the closeness to be defined more precisely later. The function $r_{NN}(\mathbf{s})$ can likely most conveniently be designed and estimated through the means of neural networks. To establish it, one can start from the assumption that a set of M input and output training signals across both pulses are available, i.e.

$$\mathbf{s}_1, \mathbf{s}_2, ..., \mathbf{s}_M \Leftrightarrow \mathbf{y}_1, \mathbf{y}_2, ..., \mathbf{y}_M \tag{4}$$

and

$$\hat{\mathbf{s}}_1, \hat{\mathbf{s}}_2, ..., \hat{\mathbf{s}}_M \Leftrightarrow \hat{\mathbf{y}}_1, \hat{\mathbf{y}}_2, ..., \hat{\mathbf{y}}_M. \tag{5}$$

Each signal realization of R complex entries containing a number of targets arbitrary placed in range with random reflection values and random Doppler shifts. The frequency shift selected arbitrary from a uniform distribution constrained between $\nu_l \in [-D_{\max}, \ D_{\max}]$. The targets parameters are otherwise identical across $\mathbf{s}_l$ and $\hat{\mathbf{s}}_l$ for a given l, $1 \leq l \leq M$. Training under smaller values of $D_{\max}$ is likely to make the network less tolerant to larger frequency shifts, however, the network may process better abilities to handle targets on the smaller Doppler range space it has been trained for. For the training process one can further presume that the noise floor level is more or less constant and random target placement is likely to ensure that the networks adopts linearity of the MF process. To formally construct the link

$$\mathbf{s}_1, \mathbf{s}_2, ..., \mathbf{s}_M \Rightarrow \dot{\mathbf{y}}_1, \dot{\mathbf{y}}_2, ..., \dot{\mathbf{y}}_M \tag{6}$$

through $r_{NN}(\mathbf{s})$ a machine learning training process can be initiated to minimize the mean square error over the available data set: $r_{NN}(\mathbf{s}) = \arg\min_{\dot{r}_{NN}} \sum_{l=1}^{M} ||\dot{r}_{NN}(\mathbf{s}_l) - \hat{\mathbf{y}}_l||^2$.

2.1. Neural network structure

The input $\mathbf{s}$ and output $\hat{\mathbf{y}}$ data of the neural network is complex valued and needs to be treated accordingly. We propose to use modified versions of fully connected feed-forwarding neural networks as discussed in [13]. Particularly, the construction 1) splits complex data in real and imaginary parts 2) adopts maximum absolute normalization. The input to the first layer of the neural network will thus be $\tilde{\mathbf{s}}_l = \frac{1}{\alpha}[\Re(\mathbf{s}_l)\ \Im(\mathbf{s}_l)] \ \in \mathbb{R}^{2R}$ where $\alpha = \max\left(\ |\Re(\mathbf{s}_l)|,\ |\Im(\mathbf{s}_l)|\ \right)$, i.e. the maximum absolute value of either the real or imaginary elements of $\mathbf{s}_l$. The output from the network will consist of $2R$ real entries who are combined together to form complex values and scaled up by factor α. This can be completed outside the network. Experimenting with various sizes indicates that even networks with one hidden layer and the same number of nodes as input samples can yield very acceptable performance for MF outcomes, as will be shown.

3. SIMULATED EXAMPLES

This section demonstrates the laid out principles on some concrete examples and provides detailed simulation results. The examples are founded upon a baseband modeled radar, $f_0 = 0$ with a sampling rate of $f_s = 25$kHz. The radar is set to cover a simulated range of $R = 300$ bins where the pulse $\mathbf{p}$ has a bandwidth of $\Delta f = 8$kHz over a duration of $L = 26$ range bins. From reflections based on $\mathbf{p}$ the objective will be to reconstruct MF output resembling either one of two higher resolution waveforms. The two high resolution pulses are defined as T1 and T2. The T1 pulse, $\Delta\hat{f} = 10$kHz, approximates a modest waveform bandwidth increase of 2kHz while T2 adds a total of 4kHz leading to $\Delta\hat{f} = 12$kHz. All pulses have otherwise identical norm. For reference, figure 1 displays the real and imaginary parts of the three pulses.

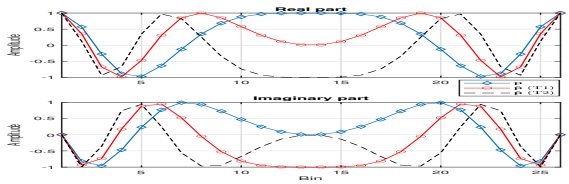

Fig. 1: Real and imaginary parts of simulated waveforms.

Dette er en postprint-versjon/This is a postprint version.
DOI til publisert versjon/DOI to published version: 10.1109/ICASSP49357.2023.10095034

To construct a training database a set of signals were generated with randomly selected, either two or three targets, with random reflection values and random Doppler with up to 10% (800Hz) shift in the frequency in either direction. The range position of the targets was determined randomly and the noise floor was set at -25dB. $M = 100000$ such signals were generated under $\mathbf{p}$ and $\hat{\mathbf{p}}$. The MF pulses on receiving ends were assumed tapered with the Chebyshev window with 100dB sidelobe attenuation. The set was put to use to train two fully connected neural networks with 600 real input and output values and 600 nodes and only one single hidden layer with $tanh$ as the node activation function. The full data set was used for training using the scaled conjugate algorithm over 100000 epochs. The application of $tanh$ in the nodes should be able to provide a dynamic range of about 40dB depending on numerical precision [13]. As an alternative, the signal may be split in parts for processing or [9] may be consulted.

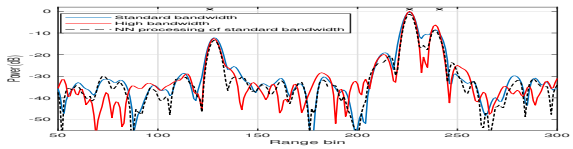

Fig. 2: Magnitude: MF and NN processing (T1).

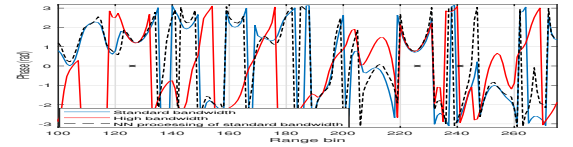

Fig. 3: Phase: MF and NN processing (T1).

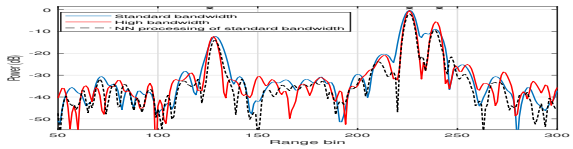

Fig. 4: Magnitude: MF and NN processing (T2).

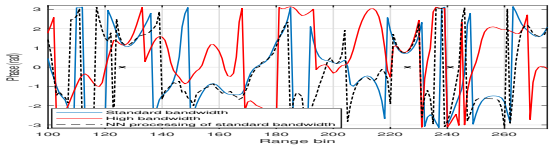

Fig. 5: Phase: MF and NN processing (T2).

3.1. Single pulse characterization

Figure 2 presents a typical example of a training signal with the blue curve showing the magnitude outcome of MF with $\mathbf{p}$ while the red line demonstrates the transmission and MF reception with $\hat{\mathbf{p}}$ (T1). The targets after MF are located at range bins 125, 225 and 240 and are marked with a cross at top. The leftmost target is Doppler shifted -800Hz while the rightmost is shifted 800Hz. No Doppler shift is imposed on the middle target. This exact signal was not used for training and the black dotted curve demonstrates the output from the trained neural network for T1. Visually, the outcome from the neural network closely matches the red higher bandwidth MF with very identical narrower mainlobes while the sidelobes roughly follow the structure of the original $\mathbf{p}$ waveform. The major downside can be related to lower SNR gains with a small loss of about 0.5dB for the first two targets compared to the high bandwidth waveform. The third target does not experience any noticeable SNR reduction. The ability to separate the two right targets is clearly enhanced by the neural network even though it is not up to the same level if $\hat{\mathbf{p}}$ had been applied for transmission. In any case, an exact replication can not be expected. For coherent processing it is essential that the phase of the processed signal is preserved; this is displayed in figure 3 and the phases all converge towards the same values at target locations.

Pulse	Peak power (dB)	Peak sidelobe (dB)	3dB width (bins)
$\mathbf{p}$	0.1535	-18.70	5.52
$\hat{\mathbf{p}}$ (T1)	0.0327	-19.91	4.52
NN (T1) on $\mathbf{p}$	-0.7026	-19.15	4.54
$\hat{\mathbf{p}}$ (T2)	-0.0140	-20.74	3.74
NN (T2) on $\mathbf{p}$	-1.2459	-23.32	3.89

Table 1: Numerical comparative figures

Figures 4 and 5 display identical results but for the T2 pulse. The network is now supposed to yield a higher resolution outcome close to the sampling limit. The ability to separate the targets is now better though there is more dynamic range variation in the neural network processed signal with several instances of deep nulls compared to figure 2. A moderate bandwidth expansion through neural networks is less likely to introduce such artifacts, however, in both instances the original sampling rate is sufficient to avoid aliasing. Table 1, assuming a single target with unit reflection energy and noise level of -25dB, provides exact numerical results for the peak gain value, peak first sidelobe and the half-power width in range bins using spline interpolation. The sidelobes from the networks are not symmetric and the largest value to the left or right is provided. The networks not only return a narrow mainlobe but the first sidelobe is also slightly lower; the overall processing loss is thus minor.

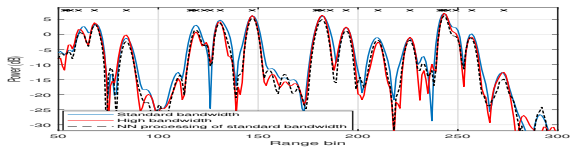

Fig. 6: Magnitude: MF and NN processing (T1).

To supplement previous plots, figures 6 and 7 demonstrate the outcomes when 30 zero Doppler targets are positioned randomly in range with varying distance and random reflecitivity values. Note that the networks were only ever trained on scenarios with no more 3 targets at once but have

Dette er en postprint-versjon/This is a postprint version.
DOI til publisert versjon/DOI to published version: 10.1109/ICASSP49357.2023.10095034

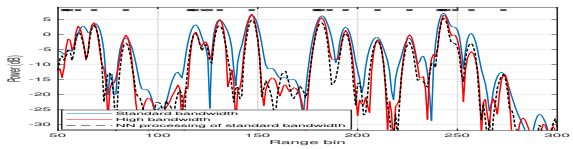

Fig. 7: Magnitude: MF and NN processing (T2).

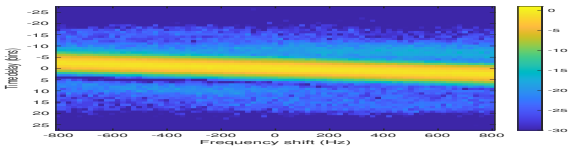

Fig. 8: Delay-Doppler diagram from NN (T1).

managed to generalize themselves to yield very comparable outcomes as standard MF and the NN magnitudes exhibit high degree of alignment towards T1 and T2. On average, the peak target SNR loss between the real high bandwidth pulse and the neural network result amounts to 0.5186dB for targets in figure 6. The mean difference increases to 0.9426dB for targets in figure 7 as bandwidth extrapolation readjusts SNR levels leading to a greater trade-off.

3.2. Delay-Doppler characterization

Radar pulses are often characterized using the ambiguity function to evaluate their performance as the targets exhibit shift in Doppler and range. Processing the signals through neural networks can alter the original properties and, as already discussed, the training should be carried out over a defined target Doppler interval to make certain the network learns these attributes. Figure 8 shows the resulting delay-Doppler figure when the neural network is applied on signals consisting of low bandwidth waveform $\mathbf{p}$. The mainlobe is narrow as if the T1 pulse had been applied with slightly lower peak values while the sidelobe spread features similar behavior as of the original waveform. Overall, the result is a managed compromise and the properties of the LFM pulse with regard to delay and Doppler are sustained.

Figure 9 shows the analogous results for the T2 pulse. The neural network processing retains the delay and Doppler hallmarks with a narrow mainlobe, however, the sidelobes now display a marked different structure with one single dominating sidelobe which increases with Doppler.

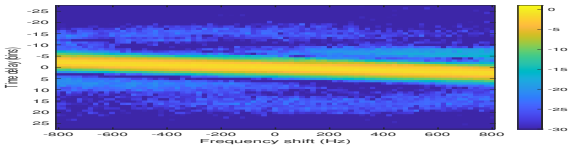

Fig. 9: Delay-Doppler diagram from NN (T2).

3.3. Detection characterization

The figures shown have demonstrated some important aspects of trained neural networks, however, to assess any advantages for radar target detection exhaustive simulations needs to be performed. For this, cell averaging (CA) - CFAR detection tests were done on low and both high bandwidth signals, T1 and T2, alongside low bandwidth signals processed via trained neural networks. The simulation scenario was set to be similar to figure 4 with 10 targets positioned randomly across range bins with reflections values set accordingly to a given SNR. Due to arbitrary placement many targets end up being close to each other and a narrow mainlobe is desirable to improve detectional capabilities. For each SNR level 100000 simulations were carried out to determine the probability of detection (Pd) and the false alarm rate (Pfa). The CA-CFAR parameters were set as 4 guard cells and 6 averaging cells on each side of cell under test (CUT) and a detection threshold of 13dB. The results are provided in figure 10 for T1 pulse and figure 11 for T2. The neural network Pd returns (black dotted curves) are very similar to if the larger wideband pulses had been transmitted and processed (red line). The Pfa is also retained at the same level in all cases. One can conclude that even though the networks may introduce SNR losses, this is compensated by the narrower mainlobes as the detection capability improves well with application of trained neural networks for the MF process.

4. CONCLUSION

Radar systems commonly oversample incoming data and a neural network based approach was presented to factor this in substituting for the standard matched filtering process. The networks were trained with an aim to provide an output approximating the utilization of a larger bandwidth pulse. This provides a new alternative approach to the construction of mismatched filters using machine learning techniques. It was shown that small fully connected feed-forwarding neural networks can be trained to return high resolution outputs with marginal reduction in processing gain. In radar detectional scenarios this can result in better detection capability.

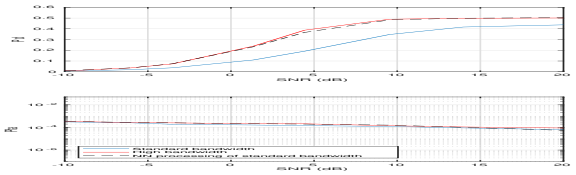

Fig. 10: Probability of detection and false alarm rate (T1)

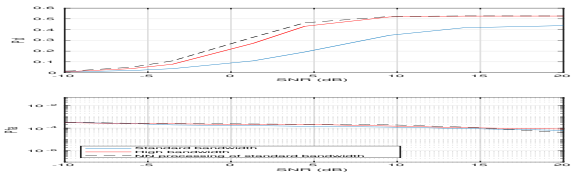

Fig. 11: Probability of detection and false alarm rate (T2)

Dette er en postprint-versjon/This is a postprint version.
DOI til publisert versjon/DOI to published version: 10.1109/ICASSP49357.2023.10095034

5. REFERENCES

[1] N. Levanon and E. Mozeson, *"Radar Signals"*, New Jersey: Wiley, 2004.

[2] M. H. Ackroyd and F. Ghani, "Optimum mismatched filters for sidelobe suppression," *IEEE Trans. Aerospace and Electronic Systems*, vol. 9, no. 2, pp. 214–218, March 1973.

[3] S. D. Blunt, K. Gerlach, and T. Higgins, "Aspects of radar range super-resolution," in *IEEE Radar Conference*, 2007, pp. 683–687.

[4] J. Kempf and J. A. Jackson, "A modified least-squares mismatched filter for use in radar applications with additive noise," in *IEEE Radar Conference*, 2020, pp. 804–809.

[5] Adrián Vega Delgado, Matilde Sánchez-Fernández, Luca Venturino, and Antonia Tulino, "Super-resolution in automotive pulse radars," *IEEE J. Sel. Areas Comm.*, vol. 15, no. 4, pp. 913–926, June 2021.

[6] K. Armanious, S. Abdulatif, F. Aziz, U. Schneider, and B. Yang, "An adversarial super-resolution remedy for radar design trade-offs," in *European Signal Processing Conference*, 2019.

[7] Ping Lang, Xiongjun Fu, Marco Martorella, Jian Dong, Rui Qin, Xianpeng Meng, and Min Xie, "A comprehensive survey of machine learning applied to radar signal processing," *arXiv preprint 2009.13702*, 2020.

[8] Z. Geng, H. Yan, J. Zhang, and D. Zhu, "Deep-learning for radar: A survey," *IEEE Access*, vol. 9, pp. 141800–141818, 2021.

[9] J. Akhtar, "Neural network LFM pulse compression," in *Proc. of IEEE Radar Conference*, 2023.

[10] P. P. Gandhi and S. A. Kassam, "Optimality of the cell averaging CFAR detector," *IEEE Trans. Inf. Theory*, vol. 40, no. 4, pp. 1226–1228, Nov. 1994.

[11] F. J. Harris, "On the use of windows for harmonic analysis with the discrete Fourier transform," *Proceedings of the IEEE*, vol. 66, no. 1, pp. 51–83, Jan. 1978.

[12] A. V. Oppenheim and R. W. Schafer, *"Discrete-Time Signal Processing"*, Prentice-Hall, 1989.

[13] J. Akhtar, "Augmenting radar Doppler resolution with neural networks," in *European Signal Processing Conference*, 2021, pp. 1551–1555.

Dette er en postprint-versjon/This is a postprint version.
DOI til publisert versjon/DOI to published version: 10.1109/ICASSP49357.2023.10095034